Analysis of electromagnetic field generated by a magnetic pulse joining machine

K. Sofi[1,2*], M. Hamzaoui[1], H. El Idrissi[2], A. Nait Sidi Moh[1], A. Hamzaoui[3]

[1]LTI, EA 3899, University of Picardie Jules Verne, INSSET, Saint-Quentin, France
[2]LEEA-TI, Hassan II University of Casablanca, FSTM, Mohammedia, Morocco
[3]LGECOS, Cadi Ayyad University, ENSA, Marrakesh, Morocco
* Corresponding author. Email: Khadija.sofi@etud.u-picardie.fr

Abstract

In magnetic pulse joining process, the principal components are the massive coil and the workpieces. In the coil-workpiece region, the magnetic field is generated by a pulsed and intense current. The welding is produced by the eddy current in the workpieces. An equivalent electrical scheme is proposed to specify the characteristics of the magnetic pulse generator. The main purpose of this article is to study the propagation of the electromagnetic fields in the coil and its propagation around the coil. The generator is modelled by an RLC circuit. The current pulse is based on experimental measurements using a Rogowski coil and integrated in the numerical simulation as an RLC circuit. Then using magnetic field theory, we measured the magnetic field around the coil using a flux loop and by introducing an analytical model of a massive one turn coil transformed into a multi-turn one. The analytical model is based on mutual inductance between two coaxial circular coils. A 3D numerical simulation using the finite element method and electromagnetic solver in ls-dyna software is developed to calculate the current distribution in the coil. The current density given by numerical analysis shows how the current is insignificant in the outer corners of the massive coil. This approximation is related to the analytical model design by neglecting these corners. Finally, we proposed an experimental setup to estimate electromagnetic fields around the coil. To validate the analytical method and using a massive one turn coil, we performed experimental measurements of magnetic flux density using an external one-turn coil.

Keywords

Modelling, Simulation, Finite Element Method, Magnetic pulse joining, Electromagnetic field.

1 Introduction

Investigating the magnetic field generated around the machine is an obligatory step in the manufacturing operation of electromagnetic deformation of metal pieces. It is an urgent need to address the safety of the generator before integrating it in an industrial environment. The magnetic pulse generator is used in many industrial applications such as welding forming and crimping of metal pieces. Magnetic pulse joining is a cold and fast welding process for both similar and dissimilar materials using an electromagnetic pulse generator (Tobergte & Curtis, 2013), (Broeckhove & Willemsens, 2010). The generator is generally represented by an RLC circuit demonstrating its simple functionality with electrodynamics equations (Psyk et al, 2011). Previous experimental research investigating the thermal behaviour in the coil of the generator shows that the temperature in the coil is generally at 34°C at a current peak of 150 kA (Sofi et al., 2017). The magnetic pulse joining method, which only operates on electrical conductive parts, exploits the eddy current induced in the workpiece by a burst of a single current pulse at a frequency of a few tens of kHz. Using high current switches called spark-gaps, the current pulse is produced by a sudden discharge of power capacitors through a massive coil of copper alloy. The level of the current can reach several tens or even hundreds of kA and produces around and into the coil a magnetic field from micro-Teslas to a few Teslas at the centre of the coil. A general process of joining two metallic tubes is shown in **Fig. 1**, during the very intense and short current pulse (Shribman, 2007) .

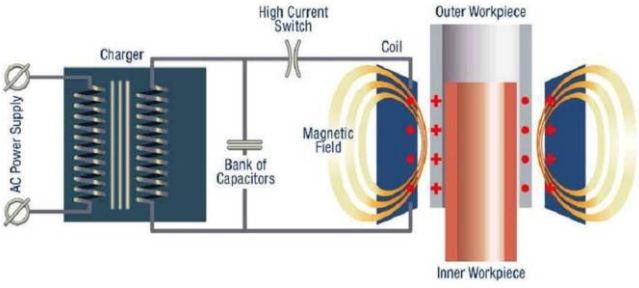

***Figure 1**: process of magnetic pulse tubes joining*

In a recent study conducted by (Mansouri et al., 2016), the magnetic field in the coil is determined by calculating the magnetic potential vector "A" using Bessel function, while other researchers have utilised the self-inductance of the coil using Grove and Smythe formulas (Zhang, 2004), (Nassiri et al., 2015) and Numerical analysis using Finite Element Method (Haiping & Chunfeng, 2009) to measure the magnetic field. To avoid long numerical simulation instead, this paper suggests an analytical design of a massive one turn coil using a multi-turn one. The number of turns is defined by skin depth related to the frequency of the current pulse in the coil. The multi-turn design of the coil is based on the geometry of the massive coil and the development of mutual inductance between two circular coils. The rest of this paper is organized as follows: in the second section, we expose the electrical scheme of the generator and the differential equation of its RLC circuit. Furthermore, we state the method of transforming a massive coil into a multi-turn one where each turn is

composed of an RL circuit using mutual inductance between circular coils and extracting the magnetic field around the coil from the mutual inductance and by introducing a flux loop as a measurement device of the field. To validate the model of the mutual inductance, we prove by a numerical analysis of current density in the coil how insignificant is the current in the outer borders of the massive coil. To experimentally validate the results of analytical method, data for this study were collected by measuring the voltage induced in an external flux loop placed at variable distance around the main coil.

2 Method

2.1 Electrical scheme of magnetic pulse welding generator

The main electrical scheme that explain the circuit of the process is given in **Fig. 2**.

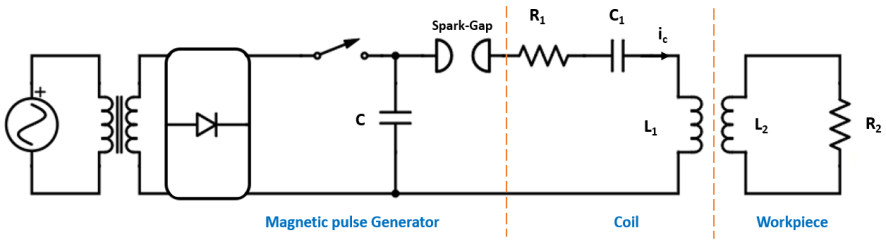

***Figure 2**: electrical scheme of magnetic pulse generator*

In **Fig. 2**, we observe a transformer operation between the coil and the tube. During experimental measurements, the coupling capacitor between the tube and the coil is insignificant due to its negligible value. The current is discharged impulsively in the coil trough Spark-Gaps which are high current switches.
In the development of the electrical machine, we consider only the electrical scheme of the coil and the discharge capacitor C as in **Eq. 1**.

$$V(t) = R_1 i_c(t) + L_1 \frac{di_c(t)}{dt} + \frac{1}{C_1}\int i_c(t)dt \tag{1}$$

where:

$$i_c(t) = C\frac{dV(t)}{dt} = C_1\frac{dV_c(t)}{dt}$$

Where L_1 represents the inductance of the coil and R_1represents the resistance of the coil. C_1 is the parasitic capacitance in the coil and i_c is the current pulse in the coil L_1. $V(t)$ and $V_c(t)$ are respectively, the voltages in the capacitor C and in the capacitor C_1.

From **Eq. 1**, we obtain the differential equations expressing the electrical behaviour of the machine in **Eq. 2.**

$$\left(1+\frac{C}{C_1}\right)\frac{dV(t)}{dt}+ R_1 C \frac{d^2V(t)}{dt^2}+ LC\frac{d^3V(t)}{dt^3}=0 \quad (2)$$

2.2 Analytical Model

In this section, we present our model of the main coil and the flux loop in order to obtain the magnetic field in the area where the generator is located. We consider a massive one turn circular coil as a multi-turn one where each turn is represented by an inductance L_i connected to a resistance R_i as shown in **Fig. 3.** A major advantage of the multi turn model is that it depends only on the geometry of the coil as explained with equations in the mutual inductance section

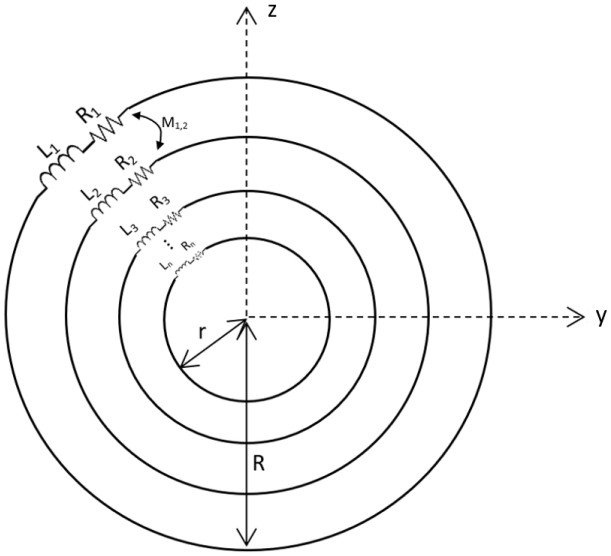

Figure 3: *representation of a massive coil by a multi-turn coil*

Using the skin depth formula developed in the magnetic field section, which depends on the frequency of the current in the coil, we define the basic number of loops as half of the length of the massive coil over the skin depth.

2.2.1 Mutual inductance of two circular coils

Using Neumann Formula of mutual inductance as expressed in **Eq. 3** between two circular coils, each loop of the coil of the **Fig. 3** is presented in **Fig. 4** by spire 1 of radius $r < a < R$. To obtain magnetic field, we used a flux loop, which is represented in **Fig. 4** by spire 2.

$$M_{12} = \frac{\mu_0}{4\pi}\oint\oint\frac{\overrightarrow{dl_1}.\overrightarrow{dl_2}}{r_{12}} \quad (3)$$

From the **Eq. 3**, the mutual inductance between two circular coaxial and parallel coils is given in **Eq. 4** (Gardiol, 2002).

$$M_{12} = \mu_0 \, k \sqrt{ab} \left[\left(\frac{2}{k^2} - 1 \right) K(k) - \frac{2}{k^2} E(k) \right] \tag{4}$$

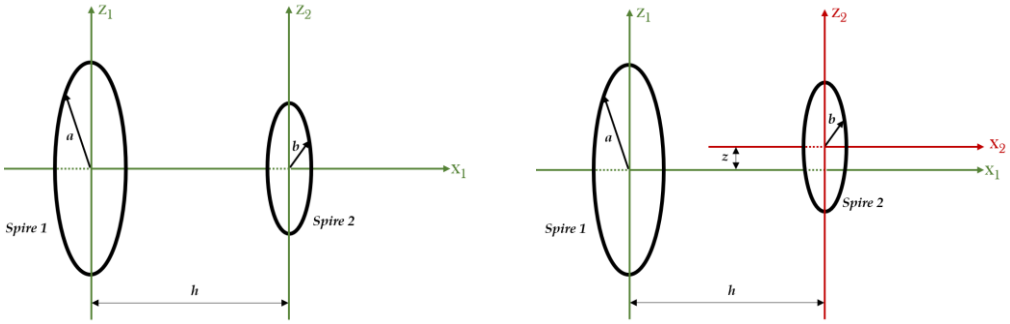

(a) (b)

Figure 4: *representation of the main coil and the flux loop, (a) coaxial loops, (b) non-coaxial.*

where E (k) and K (k) are the elliptic integrals of first and second order defined by the following equations:

$$E(k) = \int_0^{\frac{\pi}{2}} \sqrt{1 - k^2 \, sin^2\theta} \; d\theta \qquad \text{and} \qquad K(k) = \int_0^{\frac{\pi}{2}} \frac{d\theta}{\sqrt{1 - k^2 \, sin^2\theta}}$$

$$k^2 = \frac{4ab}{(a+b)^2 + h^2}$$

The mutual inductance in two non-coaxial parallel circular coils is given in **Eq. 5** (Conway, 2007)**.**

$$M_{12} = \mu_0 \pi ab \int_0^{\infty} J_0(sy) \, J_1(sa) \, J_1(sb) e^{(-s|h|)} ds \tag{5}$$

Where $J_0(x)$ is the bessel function of order 0 given by **Eq. 6**.

$$J_0(x) = \sum_{p=0}^{\infty} (-1)^p \frac{1}{2^{2p}(p!)^2} x^{2p} \tag{6}$$

2.2.2 Magnetic field

First, the number of turns n in **Fig. 3** is determined by the skin depth e formulation in **Eq. 7**.

$$e = \sqrt{\frac{2}{\omega \sigma \mu}} \tag{7}$$

The considered flux loop presents an open circuit, therefore, the current in the second coil equals to zero. Consequently, the voltage V_2 obtained by a small flux loop is given in **Eq. 8**

$$V_2 = \omega . M . I_C \quad (8)$$

And using magnetic field B, we obtain **Eq. 9**:

$$B = -\frac{\int V_2 \, dt}{S} \quad (9)$$

Considering that $S = \pi \, b^2$ represents the area of spire 2. From **Eq. 9**, magnetic field obtained by the one turn flux loop is given in **Eq. 10**

$$B = \frac{V_2}{\omega \, .S} \quad (10)$$

where ω represents the angular frequency of the current I_C,

2.3 Numerical approach

In this section, we study electromagnetic field in the coil-workpiece region based on Maxwell equations and the electromagnetic solver developed by Ls-Dyna software (Eplattenier & Çaldichoury, 2015), (Livermore Software Technology Corp, 2012).
From Gauss's law, we obtain the formulation of magnetic field and vector potential as in **Eq.11** and **Eq. 12**.

$$\vec{\mathrm{B}} = \vec{\nabla} \wedge \vec{\mathrm{A}} \quad (11)$$

$$\vec{\mathrm{B}} = \mu_0 \vec{H} \quad (12)$$

Where, $\vec{\mathrm{A}}$ the magnetic vector potential and from Ampere's law, we obtain **Eq. 13** and **Eq. 14.**

$$\vec{\mathrm{E}} = -\vec{\nabla}\varphi - \frac{\partial \vec{\mathrm{A}}}{\partial t} \quad (13)$$

$$\vec{\mathrm{J}} = \sigma \vec{\mathrm{E}} + \vec{\mathrm{J}_s} \quad (14)$$

Where φ is the electrical scalar potential, μ_0 is the magnetic permeability and σ is the electrical conductivity.
As we are using Coulomb gauge: $\vec{\nabla}\left(\sigma \vec{\mathrm{A}}\right) = 0$ and since there is no charge accumulation, we have the volume charge density $\rho = 0$.
As a result, the scalar potential verifies **Eq. 15** and **Eq. 16**. By resolving these equations, we obtain current distribution, magnetic field and Lorentz force in the coil.

$$\vec{\nabla}\left(\sigma \vec{\nabla}\varphi\right) = 0 \quad (15)$$

And

$$\sigma \frac{\partial \vec{\mathrm{A}}}{\partial t} + \vec{\nabla} \wedge \left(\frac{1}{\mu_0} \vec{\nabla} \wedge \vec{\mathrm{A}}\right) + \sigma \vec{\nabla}\varphi = \vec{\mathrm{J}_s} \quad (16)$$

Dynamic deformation of the workpiece during forming or welding is due to the magnetic loading condition, which is in this case the resultant Lorentz force (Fan, Yu, & Li, 2016). From the current distribution J, we obtain the Lorentz force in **Eq. 17** acting on the deformation of the metal piece (Kore et al, 2009).

$$\vec{F} = \vec{J} \times \vec{B} \tag{17}$$

2.3.1 3D Modelling

Numerical simulation was performed in order to validate the process of the analytical model. Using finite element method representation, the 3D model of the massive coil used in experimental measurement is shown in **Fig 5**.

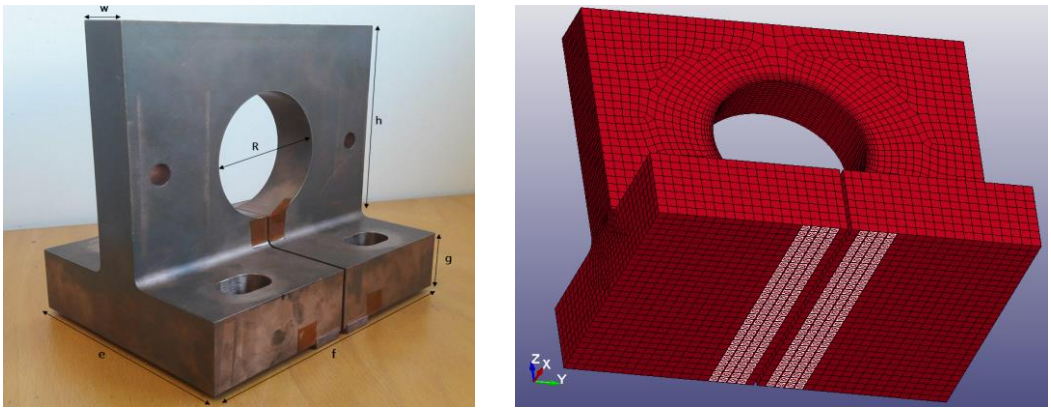

(a) ***(b)***

Figure 5: *3D representation of the welding coil, (a) real coil, (b) 3D model*

The massive coil is made of a copper alloy (SICLANIC Copper Alloy) and the holes in **Fig. 5 (a)** are used to fix it and also to fix workpieces. In the 3D model represented in **Fig. 5 (b)**, the coil is made of 35240 Hexahedrons and boundary conditions are specified only in the white bars, these bars represent the input and output of the current.
The material parameters are given in **Table 1**, while dimensions of the coil are stated in **Table 2**.

Material	Mass density (kg/m^3)	Young's modulus (Pa)	Poisson's ratio
Siclanic	$8.900e^3$	$1.30e^{11}$	0.29

Table 1: *Material parameters*

e (mm)	f (mm)	g (mm)	h (mm)	R (mm)	w (mm)
150	200	40	140	80	30

Table 2: *Coil dimensions*

2.3.2 Simulation results

During numerical simulations, we noticed the same behavior of the current density, magnetic field and Lorentz force for current pulses with different current peak. Therefore, we chose the current *I* used during this simulation as presented in **Fig. 6.**

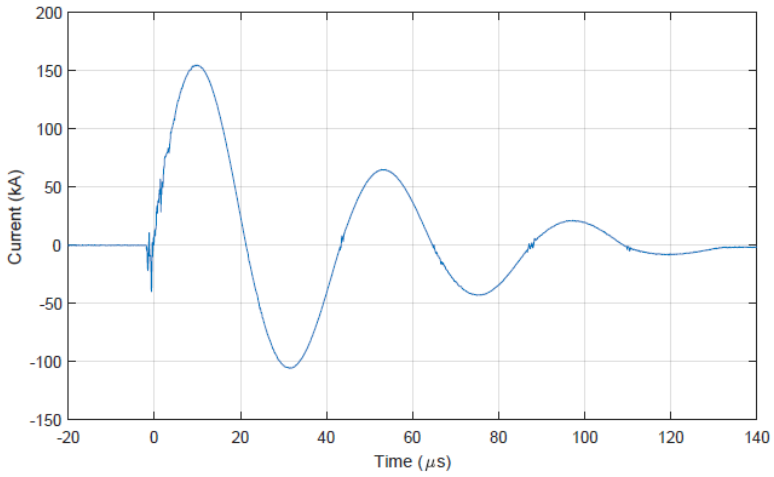

Figure 6: *Current pulse in the coil*

Performed numerical simulations gives the results of **Fig. 7** about the current density in the coil at a current *I=150kA*.

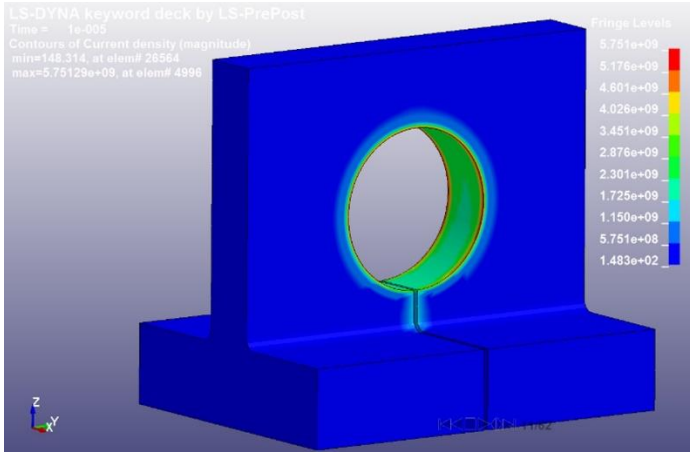

Figure 7: *current distribution in the coil during the pulse*

Fig. 7 shows how the current circulates essentially in the periphery of the inner circle of the coil ($J = 5.75e^9\ A/m^2$) while it's insignificant in the outer borders ($J = 1.48e^2\ A/m^2$). During the current pulse, we obtain magnetic field H and Lorentz force density F at $R/2 = 40\ mm$ as shown in **Fig. 8** and **Fig. 9**.

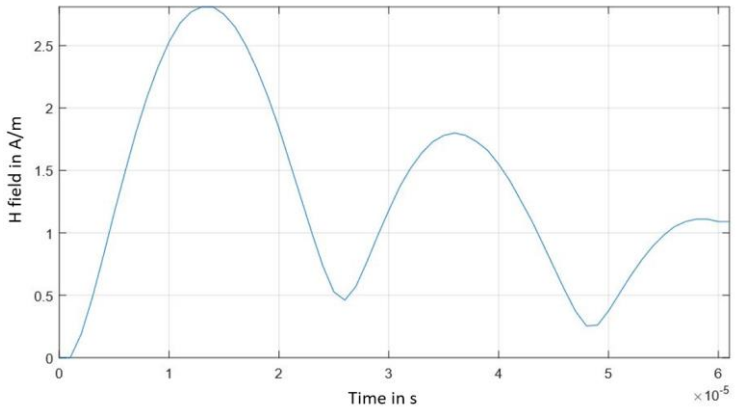

Figure 8: *Magnetic field magnitude induced by the massive coil*

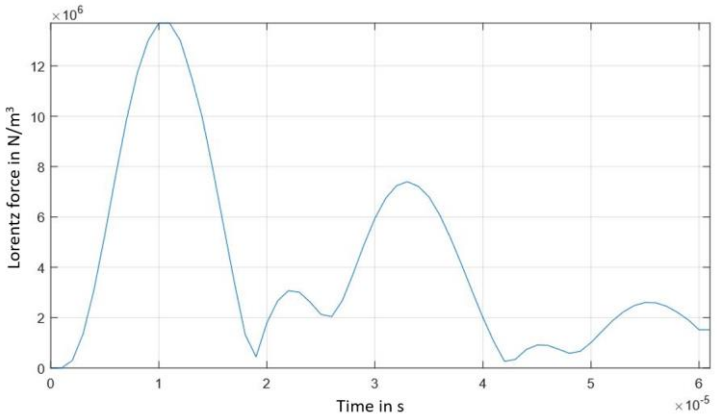

Figure 9: *Lorentz force magnitude*

At *10 µs*, the current peak is equal to *150 kA* which corresponds in **Fig. 8** to a magnetic field H of *2.75 A/m* and in **Fig. 9** to the Lorentz force density of 14.10^6 N/m^3. This density of Lorentz force can deform a metal workpiece inside the coil.
As shown in **Fig. 8** and **Fig. 9**, the two first big bumps in magnetic field and Lorentz force correspond to maximum and minimum current magnitude, while the small bumps are produced when *I=0 A*. This result is explained by the presence of magnetization and hysteresis phenomena in the coil. Furthermore, Lorentz force depends on *J* as stated in **Eq. 17.** When the current is equal to zero, *J* represents the generated eddy current in the coil.

3 Analytical and experimental results

To perform analytical simulations, radius r equals to the inner radius of the coil in numerical analysis, while radius R is chosen as the maximum outer radius of the same coil. The results are obtained for a loading voltage of *2.5 kV, 5.5 kV* and *8.5 kV*. To measure magnetic field around the main coil, we connect a flux loop, of radius *6cm* and made of a copper wire, to an oscilloscope with a bandwidth of *1 GHz.*

During the experimental measurements, the flux loop was placed respectively at 1m, 1.5m and 2m from the massive coil. These distances are chosen in order to observe later the effect of the magnetic field on instrumentation equipment such as sensors used to automate welding process.

As shown in **Fig. 10,** the magnetic field is obtained at *2.5 kV* and decreases each time the distance of the flux loop from the massive coil increases. We observe similar performance at *5.5 kV* shown in **Fig. 11** and at *8.5 kV* represented in **Fig. 12**.

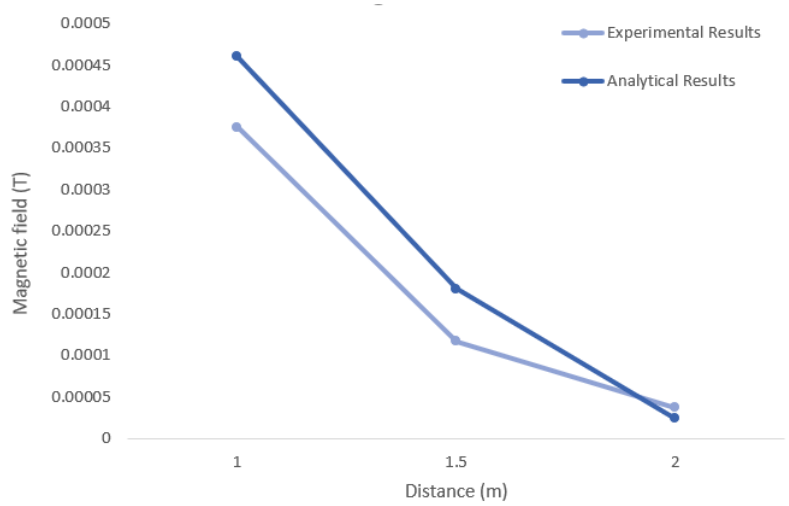

Figure 10: *Magnetic field at 2.5 kV*

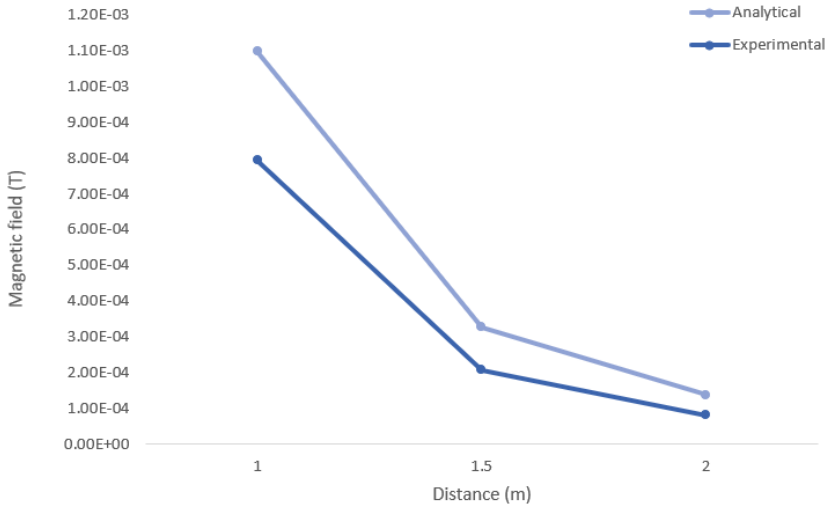

Figure 11: *Magnetic field at 5.5 kV*

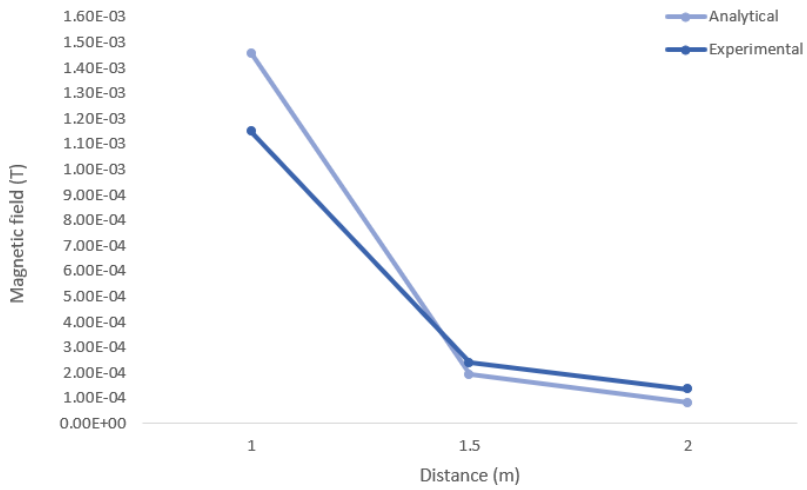

Figure 12: *Magnetic field at 8.5 kV*

The magnetic field increases respectively with the voltage as performed in analytical and experimental measurements. At the distance *1m*, we measured a magnetic field *0.36 mT* at *2.5 kV* to *1.15 mT* at *8.5 kV*.

The approximation between the analytical model and the massive coil in numerical simulation is due to the concentration of current density distribution in the center of coil. This result is likely the source of the similarity of experimental and analytical results. This is explained from the current density in the outer corners of the massive coil, which has very small values compared to the current density in the center (10^2 $A.m^{-2}$ in the corners and 10^9 $A.m^{-2}$ at the center).

4 Conclusion

The main goal of the current study was to examine magnetic field generated around the electromagnetic joining machine. The principal theoretical implication of this work is that an analytical model using a multi-turn coil can replace a massive one turn coil in terms of the produced magnetic field around it. Experimental setup was designed to measure magnetic field around the massive coil using a flux loop. These experiments confirm the analytical results of magnetic field. Furthermore, numerical simulations of current distribution were presented in this study. By comparing high current density in the inner circle of the coil to the lower values of the same current density in the outers borders, these findings suggest that a massive one turn coil may be designed analytically using a multi-turn one and avoid heavy numerical simulations. This research provides a framework for the exploration of electromagnetic field generated by a magnetic pulse machine, which will serve in defining the effect of the machine in an industrial environment on instrumentation equipment and to calculate analytically the Lorentz force applied on workpieces of different materials.

Acknowledgments

We gratefully thank Hauts-de-France Region and Innovaltech Plateform for financial and material support.

References

Broeckhove, J., & Willemsens, L. (2010). *Experimental research on magnetic pulse welding of dissimilar metals*.

Conway, J. T. (2007). Inductance calculations for noncoaxial coils using bessel functions. *IEEE Transactions on Magnetics*, *43*(3), 1023–1034. https://doi.org/10.1109/TMAG.2006.888565

Eplattenier, P. L., & Çaldichoury, I. (2015). Recent developments in the Electromagnetic Module : a new 2D axi-symmetric EM solver, (4).

Fan, Z., Yu, H., & Li, C. (2016). Plastic deformation behavior of bi-metal tubes during magnetic pulse cladding: FE analysis and experiments. *Journal of Materials Processing Technology*, *229*, 230–243. https://doi.org/10.1016/j.jmatprotec.2015.09.021

Gardiol, F. E. (2002). *Electromagnétisme*. Presses polytechniques et universitaires romandes. Retrieved from https://books.google.fr/books?id=AUl0p5tmXSYC&pg=PA284&lpg=PA284&dq=inductance+mutuelle+entre+deux+spires+f+gardiol&source=bl&ots=zBHVG9SBNq&sig=5kiTsAnOB5bhjKRRdzWqRXv1mF0&hl=fr&sa=X&ved=0ahUKEwjXrfHy3d_ZAhWHr6QKHfj6B3UQ6AEIKDAA#v=onepage&q=inductance mutuelle entre deux spires f gardiol&f=false

Haiping, Y. U., & Chunfeng, L. I. (2009). Effects of current frequency on electromagnetic tube compression. *Journal of Materials Processing Technology*, *209*(2), 1053–1059. https://doi.org/10.1016/j.jmatprotec.2008.03.011

Kore, S. D., Imbert, J., Worswick, M. J., & Zhou, Y. (2009). Electromagnetic impact welding of Mg to Al sheets. *Science and Technology of Welding and Joining*, *14*(6), 549–553. https://doi.org/10.1179/136217109X449201

Livermore Software Technology Corp. (2012). EM THEORY MANUAL - Electromagnetism and Linear Algebra in LS-DYNA.

Mansouri, O., Sup, E., Maloberti, O., Sup, E., & Maloberti, O. (2016). Analytical 1D-calculation of a 1-turn Coil Parameters for the Magneto-Forming Technology Analytical 1D-calculation of a 1-turn Coil Parameters for the Magneto-Forming Technology. https://doi.org/10.17877/DE290R-16975

Nassiri, A., Nassiri, A., Campbell, C., Chini, G., & Kinsey, B. (2015). Analytical Model and Experimental Validation of Single Turn , Axi-Symmetric Coil for Electromagnetic Forming and Welding An alytical Model and Experimental Validation of Single Turn , Axi - Symmetric Coil for Electromagnetic Forming and Welding. *Procedia Manufacturing*, *1*(May), 814–827. https://doi.org/10.1016/j.promfg.2015.09.070

Psyk, V., Risch, D., Kinsey, B. L., Tekkaya, A. E., & Kleiner, M. (2011). Electromagnetic forming - A review. *Journal of Materials Processing Technology*, *211*(5), 787–829. https://doi.org/10.1016/j.jmatprotec.2010.12.012

Shribman, V. (2007). Magnetic pulse welding of automotive HVAC parts. *Rapport Technique, Pulsar Ltd*, *8*, 41–42. Retrieved from http://www.magpulse.co.in/pdf/1.welding/applications/7.others/MPW for HVAC.pdf

SICLANIC Copper Alloy. (n.d.). Retrieved March 9, 2018, from http://www.matweb.com/search/DataSheet.aspx?MatGUID=c449faa3b0334af19a6e68f7cc817ee5&ckck=1

Sofi, K., Idrissi, H. E. L., Hamzaoui, M., Hamzaoui, A., Alaoui, L. C., Jouaffre, D., … Modelization, A. (2017). current and temperature distribution in a massive one turncoil used in electromagnetic pulse generator. *18th International Symposium on Electromagnetic Fields in Mechatronics, Electrical and Electronic Engineering (ISEF) Book of Abstracts*, 5–6.

Tobergte, D. R., & Curtis, S. (2013). High Speed Forming 2014. *Journal of Chemical Information and Modeling*, *53*(9), 1689–1699. https://doi.org/10.1017/CBO9781107415324.004

Zhang, P. (2004). Analysis of the Electromagnetic Impulse Joining Process with a Field Concentrator. *AIP Conference Proceedings*, *712*(2004), 1253–1258. https://doi.org/10.1063/1.1766701